

# Confronting $\Lambda$ CDM with Gravitational Lensing Constraints on Small Scale Structure

R. Benton Metcalf<sup>1</sup>

*Department of Astronomy and Astrophysics, University of California, Santa Cruz, CA 95064 USA*

## ABSTRACT

This paper primarily addresses the question of whether recent lensing observations probing the small scale structure in the universe are consistent with the  $\Lambda$ CDM model. A conservative approach is taken where only the most difficult to explain cases of image flux anomalies in strong lenses are considered. Numerical simulations are performed to compare predictions for the  $\Lambda$ CDM small scale mass function with observed flux ratios. It is found by simulating several represent cases that all the cusp caustic lens anomalies and the disagreements between monochromatic flux ratios and simple lens models might be explained without any substructure in the primary lenses' dark matter halos. Intergalactic  $\Lambda$ CDM halos are enough to naturally explain these cases. However, thus far, spectroscopic gravitational lensing observations require more small mass halos ( $\sim 10^6 M_\odot$ ) than is expected in the  $\Lambda$ CDM model.

## 1. Introduction

The Cold Dark Matter (CDM) model predicts a large quantity of small mass dark matter halos ( $\lesssim 10^7 M_\odot$ ) that must have little or no stars in them to agree with the number counts of dwarf galaxies. Quasars (QSOs) that are being gravitationally lensed into multiple images have recently been used to put limits on the surface density and mass of such invisible subclumps (Mao & Schneider 1998; Metcalf & Madau 2001; Chiba 2002; Metcalf 2002; Metcalf & Zhao 2002; Dalal & Kochanek 2002; Bradač et al. 2002; Keeton 2003; Metcalf et al. 2004). Small mass clumps near the images affect the observed magnifications ratios. The question arises as to whether these observations are compatible with the current  $\Lambda$ CDM model.

This question is significantly complicated by the fact that all lenses were not created equal. Some lenses provide much stronger and more certain constraints on the small scale structure than others. In this paper, I try to take a conservative approach and consider only the lenses that provide clean, relatively unambiguous constraints. I also refrain from doing a formal likelihood analysis to constrain structure formation parameters because I think this would be premature considering the uncertainties in the relevant  $\Lambda$ CDM predictions and the small amount of data at this time.

In this paper, the single large lens that is causing the QSO to have multiple images is referred to alternately as the primary lens, the host lens or the host halo. The additional small scale halos are referred to as subhalos or substructures even if they are not physically inside the host halo, but in intergalactic space. For the purposes of this paper the standard  $\Lambda$ CDM cosmological model will have the cosmological parameters  $\Omega_m = 0.3$ ,  $\Omega_\Lambda = 0.7$ ,  $\sigma_8 = 0.9$ ,  $H_o = 70 \text{ km s}^{-1} \text{ Mpc}^{-1}$  and a scale free initial power spectrum.

In section 2, the predictions of the  $\Lambda$ CDM model are discussed. Relevant background information about strong gravitational lensing and the techniques used to probe substructure

---

<sup>1</sup>Hubble Fellow

are reviewed in section 3. A brief summary of relevant observations is in section 4. Section 5 provides a description of the lensing simulations. The results of the simulations are compared with the observations in section 6 and in section 7 the importance of these results are discussed.

## 2. Expectations for $\Lambda$ CDM

Cosmological Nbody simulations predict that  $\sim 10 - 15\%$  of the mass within the virial radius of a  $10^{12} M_\odot$  halo is in substructures with  $m \gtrsim 10^7 M_\odot$  (Moore et al. 1999; Klypin et al. 1999). Cosmological simulations are limited to particle masses of  $\gtrsim 10^6 M_\odot$  so smaller substructures cannot be probed directly. For the strong lensing studies considered here, we are interested in the mass fraction in substructure at a projected radius of  $\sim 10$  kpc which may be substantially less than the value for the halo as a whole because of tidal stripping, tidal heating, and dynamical friction. Limited resolution can make overmerging a problem at these radii. The lensing observations are also sensitive to substructure masses well below the resolution of the simulations. In addition, baryons may play a significant role in determining the structure of the halo at these small radii and no simulation has yet fully incorporated them at high enough resolutions. As a result of these complications, the predictions of  $\Lambda$ CDM as they pertain to substructure in strong lenses are not certain. They must be extrapolated from the simulations of insufficient resolution.

Mao et al. (2004) have done Nbody simulations in an effort to determine the level of substructure. They find that  $\lesssim 0.5\%$  of the surface density at appropriate projected radii is in structures with  $m \gtrsim 10^8 M_\odot$ . It is uncertain how accurate this estimate is since no thorough convergence tests have been done in this regime. In addition, below this mass dynamical friction becomes considerably less effective (see Taylor & Babul 2001, 2004). Dynamical friction erodes the orbits of large satellite halos, causing them to be destroyed as they sink to the center of their host halo. De Lucia et al. (2004) have also studied halo substructures for masses  $\gtrsim 10^9 M_\odot$  and find that the mass function is independent of the host halo mass.

Zentner & Bullock (2003) have developed a method for extrapolating the results of Nbody simulations to smaller masses and radii. Using their figure 19 it can be estimated that the fraction of the surface density in satellites of mass  $10^5 M_\odot < m < M_{\text{sat}}$  is

$$f_{10\text{kpc}} \simeq 0.01 \left( \frac{M_{\text{sat}}}{10^9 M_\odot} \right)^{0.5} \quad (1)$$

(for  $10^6 M_\odot \lesssim M_{\text{sat}} < 10^9 M_\odot$ ) at a projected radius of 10 kpc which is appropriate for the strong lenses considered here. Almost all of these subhalos are more than 30 kpc – or several times the typical Einstein radius – from the center of the host halo in 3 dimensions. Analytic models have also been constructed by Taylor & Babul (2004) who claim that Nbody simulations may be suffering from overmerging at small halo-centric radii (see also Taylor, Silk, & Babul 2004). They argue that because of this the above might underestimate the substructure mass function by a factor of several. However, they do not provide a prediction that can be easily compared to the lensing. For definiteness, equation (1) will be considered the  $\Lambda$ CDM predication for substructure inside the primary lens in this paper. In this sense the Nbody results, and extrapolations of them, are taken at face value although it is still possible that these simulations do not accurately reproduce the  $\Lambda$ CDM model in this regime. For example, the role of baryons is not taken into account.

In addition to the substructure inside the host lens there are also independent halos in intergalactic space that happen to be well aligned with the source, lens and observer. The number of these halos can be calculated straightforwardly using the Press-Schechter (Press & Schechter 1974) method and the Sheth-Tormen (Sheth & Tormen 2002) modification to it. A typical line of sight to  $z = 2$  passes within  $1/3$  of the virial of 150 halos of mass  $10^5 M_\odot < m < 10^9 M_\odot$ . Since the deflections from these halos will add, they can make a contribution to the lensing that is significantly larger than one halo could do by itself. We will see that they have an important effect on the magnification of any small source at high redshift.

Besides the mass function of halos one must also consider how the concentration of the halos depends on mass. The Nbody simulations are generally not of high enough resolution to determine the concentration of halos with masses below  $\sim 10^9 M_\odot$  that are inside the halos of large galaxies. Some progress can be made in this regard by dropping “live” artificially constructed satellites into a static model for the host halo extracted from a cosmological simulation (as in Hayashi et al. 2003). The subhalos are taken to have Navarro, Frenk & White (NFW) profiles (Navarro, Frenk, & White 1997)

$$\rho(r) = \frac{r_s \rho_o}{r(1 + r/r_s)^2} \quad (2)$$

The simulation results indicate that substructures are effectively tidally truncated at some radius with the interior remaining relatively unmodified until the stripping radius becomes on the order of the scale length,  $r_s$ . This is the simple picture that will be used for the simulations in this paper. By extrapolation of Nbody simulations Zentner & Bullock (2003) find that the concentration of small halos goes as

$$c \equiv \frac{r_{\text{vir}}}{r_s} \simeq c_o \left( \frac{m_{\text{vir}}}{10^{12} M_\odot} \right)^{-\beta} \quad (3)$$

with  $c_o \simeq 12$  and  $\beta \simeq 0.10 - 0.15$ . In this paper  $\beta = 0.13$  is adopted.  $m_{\text{vir}}$  is the virial mass of the subhalo before it is tidally stripped.

### 3. Some Lensing Background

Some background on strong gravitational lensing will be necessary to understand the results that follow. For a more complete description see Schneider, Ehlers, & Falco (1992), or any other review of strong lensing (see Saha & Williams (2003) for a nice qualitative description). A strong lens can be defined as one where there are multiple images of a single source. For any lens – that is less concentrated than a perfect point mass – there will be one image if the source is far enough away from the center of the lens. On the source plane of a potential strong lens there are also regions where there are three images and, when the lens is not perfectly axisymmetric, five images. One of these images is usually near the very center of the lens and, if the density profile is very cuspy there, this image is highly demagnified; in the large majority of cases it is not observed (for an exception see Winn, Rusin, & Kochanek 2004). This leaves two or four images. Separating these regions on the source plane are the caustic curves. If the source moves from outside a caustic to the inside of it two images are created. Generally for a smooth centrally concentrated lenses there are two caustic curves – termed the radial and tangential caustics.

Figure 1 illustrates the basic configurations for four image lenses. In this figure the central (or tangential) caustic is shown as a solid curve and the critical curve that is the image of

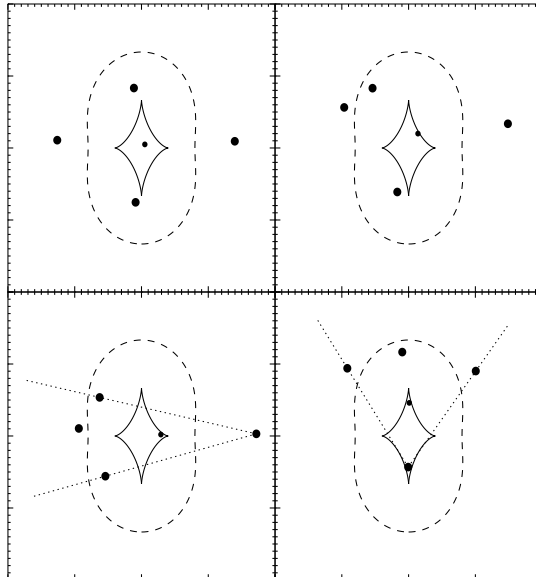


Fig. 1.— Four basic lens configurations. In each case the caustic is shown as a solid curve and the critical curve is shown as a dashed curve (only one of each for each configuration is shown). The four images that are usually observable are shown as large dots and the source position is marked by a small dot. On the top left is the *Einstein cross* configuration where all the images are well separated and the source is near the center of the lens which is at the center of each plot. On the top right is the *fold caustic* configuration where two of the images are close together and the source is near the caustic, but not near a cusp. The lower left shows a *short axis cusp caustic* configuration and the lower right is a *long axis cusp caustic* configuration. The *image opening angle* is the angle between the dotted lines shown in the cusp caustic cases. Note that this opening angle is defined differently here than it is in some other papers where the center of the lens is taken as the vertex. There are always two images within the critical curve where the magnification is negative and two outside of the curve where the magnification is positive. The long and short axis cusp caustic cases differ in that the close triplet of images have either one (long axis) or two (short axis) negative images. They also differ in how close the singlet image is to the center of the lens which can usually be determined observationally.

the caustic curve is shown as a dashed curve. Images within the dashed curve have negative magnification reflecting the fact that these images are reversed in one dimension with respect to images that are outside the curve (i.e. negative parity in one dimension). The two types of cusp caustic configurations differ in that for the long axis case the triplet of close images includes one of these negative images and in the short axis case it includes two. The sign of the magnifications is not directly observable, but for configurations other than Einstein crosses one can usually deduce them because the parities alternate from image to image as one follows the critical curve and the positive parity images are generally further from the center of the lens. For example, the two types cusp caustic configurations can be distinguished by how close the singlet image is to the center of the lens. To measure the degree of “cuspyness” the image opening angle is defined as shown in figure 1.

To investigate the presence of substructure in a strong lens one must find a prediction that is not strongly dependent on the macroscopic form of the lens which is not known in detail. The magnification ratios are influenced by substructure (Metcalf & Madau 2001), but their values are model dependent which limits their use somewhat and makes their interpretation ambiguous. There are a few observables that are relatively unambiguous. They are discussed below.

### 3.1. The cusp caustic relation

It can be proven by expanding the lensing map to third order in the angular separation from a cusp in the caustic that the magnifications of the close triplet of images should sum to zero (Schneider & Weiss 1992). To make this prediction independent of the intrinsic luminosity of the QSO the images in the triplet are labeled A through C and the cusp caustic parameter,  $R_{\text{cusp}}$ , is defined as

$$R_{\text{cusp}} \equiv \frac{\mu_A + \mu_B + \mu_C}{|\mu_A| + |\mu_B| + |\mu_C|} \quad (4)$$

which should be zero if the expansion of the lens map about the cusp is valid. Small scale structure on approximately the scale of the image separations will cause  $R_{\text{cusp}}$  to differ from zero fairly independently of the form of the rest of the lens. By adding radial modes to analytic lens models Keeton, Gaudi, & Petters (2003) showed explicitly that, for their family of lens models,  $R_{\text{cusp}}$  is always small when the image opening angle is small and there are no large fluctuations in the surface density on the scale of the image separations.

Note that by the definition of  $R_{\text{cusp}}$  used here it can be both negative and positive (some authors use the absolute value of  $R_{\text{cusp}}$ ). Substructure is more likely to reduce the absolute magnification than to increase it for negative magnification images (Metcalf 2001; Metcalf & Madau 2001; Schechter & Wambsganss 2002). The positive parity images are biased in the other direction. As a result, the probability distribution of  $R_{\text{cusp}}$  will be skewed toward positive values. We will see that this is a strong effect. Also note that  $|R_{\text{cusp}}| < 1$  by definition.

Cusp caustic systems also have the benefit that the time delays between the images of the triplet are usually small, smaller than typical time scales for the variations in the radio or infrared emission. This makes the interpretation of the flux ratios as magnification ratios more secure.

### 3.2. Spectroscopic gravitational lensing

It was proposed by Moustakas & Metcalf (2003) that much of the lens model degeneracy can be removed and the sensitivity to substructure properties improved by utilizing the fact that the different emission regions of the source QSO have different physical sizes. If the lens is smooth on the scales that bridge the sizes of the emission regions, the magnification of those regions should be the same and thus the magnification ratios should be the same. The visible and near-infrared (near-IR) continuum emission regions are small,  $\sim 100$  AU (Yonehara 2001; Wyithe, Webster, & Turner 2000; Wambsganss, Schneider, & Paczynski 1990), and their magnification can be affected by microlensing by ordinary stars in the lens galaxy. The broad line emission region is  $\sim 0.1$  pc in size (Kaspi et al. 2000; Wandel, Peterson, & Malkan 1999) and is less affected by microlensing in most cases. The radio and mid-IR regions are  $\sim 10$  pc (Andreani, Franceschini, & Granato 1999; Wyithe, Agol, & Fluke 2002) and their magnification should be dominated by larger scales than stars. The narrow line emission region is even larger,  $\sim 100$  pc (Bennert et al. 2002). The magnification ratios in these bands and lines can be compared to constrain the mass, concentration and number density of substructures (Metcalf et al. 2004). A mismatch in the magnification ratios can be expressed by the *differential magnification ratios* (DMR) which is formed by taking the flux ratio between images for one emission region and then dividing by the flux ratio in another emission region. The DMRs will all be 1 if there is no mismatch. To further distill the information, the *spread* is defined as the difference between the largest DMR and the smallest DMR measured in magnitudes. The spread is independent of which image is

used to normalize the ratios and will be larger for larger the mismatch in the monochromatic flux ratios.

### 3.3. bent radio jets

Another idea for detecting substructure is to compare the images of a radio jet in a strong lens (Metcalf 2002). The Very Long Baseline Interferometer (VLBI) is able to image these jets at milliarcsecond resolution and in some cases can measure structures in the radio jet. Substructure can bend the jet in one image in a different way than is seen in the other images. In practice there can be some ambiguity in this kind of measurement because the curvature of the jet in one image can be magnified in another image by the host lens alone and, because of limited resolution, the curvature of a jet is not often well measured. However, the relative directions of the image curvatures can be predicted in a model independent way, i.e. the relative parities of the images can be predicted. A violation of this prediction would be an unambiguous signature of substructure. In general this kind of observation is sensitive to substructures that are small ( $m \sim 10^6 M_\odot$ ) and strongly concentrated.

## 4. Summary of Observations

At this time there are about 80 known gravitationally lensed QSOs with multiple images. A very useful resource for data on these lenses is provided by the CfA-Arizona Space Telescope Lens Survey (CASTLES)<sup>2</sup> which is tasked with doing followup observations of all close QSO lenses in the visible and near-IR. Of these prospective lenses some are two image lenses and some are cases where it has not yet been verified that there is a single QSO being multiply imaged rather than multiple QSOs. Many of these lenses have been observed only at visible wavelengths or only at radio wavelengths. Only a small minority of them have sufficient data to do a spectroscopic lensing study of them and/or are in a configuration that makes the cusp caustic relation a significant constraint.

There are several cases of particular interest here. The data and previous studies of these lenses are briefly summarized here.

### 4.1. Q2237+0305

This lens is probably the most well studied QSO lens. It is in an Einstein cross configuration with a lens redshift  $z_{\text{lens}} = 0.04$  and a source redshift  $z_{\text{source}} = 1.69$ . Microlensing by stars has been detected in this case through time variations in the magnification ratios at visible wavelengths and used to study the structure of the QSO (Irwin et al. 1989; Woźniak et al. 2000; Wyithe et al. 2000, 2002).

A spectroscopic lensing study of Q2237+0305 was done by Metcalf et al. (2004). It was found that the broad line ( $H\beta$ ), mid-infrared, radio and narrow line ( $[OIII]$ ) magnification ratios do not agree (although the mid-infrared and radio ratios do agree which is expected because of their similar size). The spread (see § 3.2) between the combined radio/mid-IR and the narrow lines is  $0.77 \pm 0.19$  mag. It is shown that if substructures are responsible for this, they must

---

<sup>2</sup>See <http://cfa-www.harvard.edu/castles/> for a summary of current data.

have a mass  $10^5 M_\odot \lesssim m \lesssim 10^8 M_\odot$  and that their surface density must be greater than 1% of the total surface density of the lens for typical assumptions about the radial profile of the lens and substructures. By comparison with equation (1) it can be seen that this is in violation of the  $\Lambda$ CDM predictions. Only substructures within the primary lens were considered in Metcalf et al. (2004). This study provides the strongest constraint on the type, mass and concentration, of the substructures that could be causing the magnification anomalies.

#### 4.2. B2045+265

This is the strongest case for a violation of the cusp caustic relation. The image opening angle is only  $25.2^\circ$  making this an extreme example. The redshifts are  $z_{\text{lens}} = 0.87$  and  $z_{\text{source}} = 1.28$  and it is a long axis cusp caustic configuration. In the radio, Fassnacht et al. (1999) get  $R_{\text{cusp}} = 0.516 \pm 0.018$  and Koopmans et al. (2003) get  $R_{\text{cusp}} = 0.501 \pm 0.035$  after 14 measurements. Koopmans et al. (2003) have demonstrated that the fluxes of the close triplet of images are varying independently at the 7% level (this is incorporated into the quoted error). They attribute this variation to scintillation within our galaxy. However, it seems unlikely that these variations are responsible for the large value of  $R_{\text{cusp}}$  since the radio, near-IR and visible measurements all agree (the CASTLES value is  $R_{\text{cusp}} = 0.506 \pm 0.013$ ).

#### 4.3. B1422+231

This is the first case publicized as a violation of the cusp caustic relation (Mao & Schneider 1998) and it has been further investigated in this regard by a number of authors (Keeton 2002; Metcalf & Zhao 2002; Bradač et al. 2002). The redshifts are  $z_{\text{lens}} = 0.34$  and  $z_{\text{source}} = 3.62$ . The configuration is a long axis cusp caustic with an image opening angle of  $61.0^\circ$  which makes it a less extreme case than B2045+265. This lens has been observed in the radio by Patnaik & Narasimha (2001) and Koopmans et al. (2003) who essentially agree on  $R_{\text{cusp}} = 0.187 \pm 0.006$  with no detectable time variation. The optical and near-IR measurements from CASTLES are in agreement with this value.

Keeton et al. (2003) showed that the violation of the cusp caustic relation in combination with the image opening angle is not in itself strong evidence for substructure. However, using explicit lens models, it has been shown that it is difficult to construct a lens model for B1422+231 that fits the image positions, resembles a realistic galaxy+halo and at the same time reproduces the magnification ratios (for example Metcalf & Zhao 2002; Evans & Witt 2003).

#### 4.4. B0712+472

This lens is a long axis cusp caustic case similar to B1422+231 in that the image opening angle is  $50.0^\circ$ , but two of its images are significantly closer together than in B1422+231. This indicates that the image is not located along the caustic cusp's axis of symmetry (theoretically this does not affect the prediction that  $R_{\text{cusp}} \simeq 0$ ). The redshifts are  $z_{\text{lens}} = 0.41$  and  $z_{\text{source}} = 1.34$ . The observed radio  $R_{\text{cusp}} = 0.26 \pm 0.02$  (Jackson et al. 1998; Koopmans et al. 2003). The visible/near-IR  $R_{\text{cusp}}$  is larger and a function of wavelength indicating that differential extinction might be important at these wavelengths (see CASTLES).

#### 4.5. bent radio jets

There are several cases where a distinct bend is visible in one or more of the jet images. One strong bend in lens MG0414+0534 is traceable to a visible dwarf companion galaxy. In addition B1152+199 has an unexplained mismatch in the image curvatures that can be explained by substructure (Rusin et al. 2002; Metcalf 2002). In this case the signal to noise in the measurement of the bend is not large and the conclusion that the bend is a result of substructures requires some assumptions about the form of the host lens. When these assumptions are made, the mass scale for the substructures is very low ( $\simeq 10^6 M_\odot$ ) and the probable number density is higher than expected in the  $\Lambda$ CDM model (Metcalf 2002). A less ambiguous system of this type could be extremely useful for studying substructure.

#### 4.6. other lenses

In addition to the above cusp caustic cases there is 1RXS J1131-1231 which has been observed by Sluse et al. (2003) in V-band, but not yet at radio wavelengths. The cusp caustic relation is significantly violated in this case ( $R_{\text{cusp}} = 0.355 \pm 0.015$  and image opening angle of  $43.0^\circ$ ), but since microlensing by stars in the lens galaxy could be important in the visible I choose not to emphasize this case. It is interesting that  $R_{\text{cusp}} > 0$  as expected from the substructure hypothesis.

There are a couple of other relevant cases of spectroscopic gravitational lensing observations. Wisotzki et al. (2003) have shown that the equivalent widths of the broad lines of HE0435-1223 are different in the different images. They attribute this to microlensing of the optical continuum emission. Interestingly, they still have difficulty fitting the broad-line flux ratios to a simple lens model. Since the narrow-line, radio or mid-IR flux ratios are not known in this case it is not possible to determine if larger scale substructure is responsible for this discrepancy. In lens SDSS J1004+4112, Richards et al. (2004) have observed changes in the C IV line profiles over a 322 day period that are not reproduced in all the images. They attribute this to microlensing of part of the broad line region by ordinary stars. Although intrinsic time variations are not yet completely ruled out as a cause of the variations, microlensing of the broad line region is particularly likely in this case because the QSO is under luminous and thus the broad line region is relatively small. Richards et al. (2004) also find time independent differences in the C IV profiles which could be caused by some larger scale substructure. Further observations of a larger emission regions would also be very revealing in this case.

It has been shown that in general the magnification ratios of gravitational lenses do not agree with simple lens models (Metcalf & Zhao 2002; Dalal & Kochanek 2002). Kochanek & Dalal (2004) showed that the negative magnification images tend to have smaller absolute magnifications than are predicted by simple lens models as is expected if substructures are causing the disagreements. The existence of this asymmetry is further supported by the fact that all of the observed  $R_{\text{cusp}}$  quoted above are greater than zero. The asymmetry for  $R_{\text{cusp}}$  is more extreme than it is for the distribution of just magnification ratios between positive and negative magnification images. Although the evidence is pretty good that these anomalies are caused by substructures, any constraints on the mass and density of the substructures derived from these cases is predicated on the host lens model that is assumed. Evans & Witt (2003) showed that some of the anomalies in non-cusp caustic cases can be explained by adding relatively large scale axial modes to the lens models. These models may not be consistent with what is expected from



other observations of galaxies and their halos, but they do illustrate the ambiguities that are inherent in deducing properties of the substructures from simple anomalies in the magnification ratios (not to be confused with the differential magnification ratios that are less ambiguous).

## 5. Simulations

Numerical simulations are performed to calculate the image magnification distributions. Analytic methods for calculating these distributions are discussed in section 5.1 where it is argued that they are not adequate for calculate the expected influence of small scale structure in the  $\Lambda$ CDM model. In this section the methods used in the simulations are briefly described.

Any massive object near the line of sight inside or outside of the primary lens could potentially contribute to the lensing signal. A plane approximation is used where the deflections caused by each object are treated as if they take place suddenly in the plane of that lens and the light follows an unperturbed geodesic between them. This is known to be a very good approximation. Given the angular position of a point on the source,  $\vec{\beta}$ , the simulations must calculate the image points,  $\vec{\theta}$ , that correspond to it. If there are  $N$  lenses these angular positions are related by

$$D_s \vec{\beta} = \vec{x}_{N+1}(\vec{\theta}) \quad \vec{x}_{j+1} = D_{j+1} \vec{\theta} - \sum_{i=1}^j D_{i,j+1} \hat{\alpha}_i(x_i) \quad (5)$$

where  $D_i$  is the angular size distance to the  $i$ th lens,  $D_{i,j}$  is the distance between the  $i$ th and the  $j$ th lens planes and  $D_s = D_{N+1}$  is the distance to the source. The deflection angle caused by the  $i$ th lens is  $\hat{\alpha}_i(\vec{x}_i)$ . Equation (5) is only valid for a flat cosmology because it assumes that  $D_{i,i+1} + D_{i+1,i+2} = D_{i,i+2}$ . We assume that this is the case in this paper.

The large number of small halos and the large range in size scales, from the size of the primary lens ( $\sim 100$  kpc) to the size of the source ( $\lesssim 0.1$  pc for the broad line emission region), make finding the images and calculating their sizes challenging and time consuming. An adaptive mesh refinement technique is used to overcome these problems. First, equations (5) are solved on a coarse grid. Minima in  $|\vec{\beta} - \vec{\beta}_s|$  are found where  $\vec{\beta}_s$  is the position of the center of the source. The grid regions are then modified to surround the minima. They can be modified in five different ways: 1) the center of the region can move, 2) it can expand or contract depending on whether the image is found to intersect with the border of the region, 3) the grid spacing can be made finer, 4) regions that are close together can join to become one region, and 5) if further refinement of the grid fails to reach sufficient accuracy, the region can be subdivided into nine equal subregions and the regions that do not contain any of the image are discarded. These modifications in the grid regions are continued until an estimated fractional accuracy in the area of each image reaches  $10^{-4}$  or smaller.

The code is tested by comparison with several simple cases that are solvable analytically. The simplest is to place a substructure and finite sized source in the center of the simulated region along with a external shear and/or a uniform background surface density. The code reproduces the analytic solutions for a point mass and a untruncated Singular Isothermal Sphere (SIS). Further tests are discussed in section 5.1. All simulations were done on a beowulf computer cluster at the University of California, Santa Cruz.

The entire lens is simulated at once in all cases. However, when the mass of the substructures is small, their number density can be very large slowing the code down. To reduce this problem

the angular range for the positions of substructures included in the calculation is made smaller for smaller masses. Limiting the range appears to have a small effect on the results ( $\lesssim 10\%$  on the magnification) if the region is kept large enough to contain over 150 subhalos per decade in mass.

For intergalactic halos the Press-Schechter formalism (Press & Schechter 1974, with the extra factor of 2) is used to calculate the mass function from which a random sample of halos is drawn. It is known that the modified mass function of Sheth & Tormen (2002) is a better fit to cosmological Nbody simulations. However, these mass functions are very close to each other for the range of halo masses used in this paper. Although the Press-Schechter mass function underestimates the number of halos in the mass range  $10^{10} - 10^{13} M_{\odot}$ , for  $m \lesssim 10^{10} M_{\odot}$  the Sheth-Tormen mass function is larger. The two mass functions are within a factor of 1.3 for  $10^6 M_{\odot} \lesssim m \lesssim 10^{10} M_{\odot}$ . Using the Press-Schechter mass function is more conservative. The structure of these halos is taken to be of the NFW form truncated at the virial radius. The initial power spectrum is taken to be scale invariant and normalized to  $\sigma_8 = 0.9$ . The concentrations of the halos are set according to equation (3).

The subclumps inside the primary lens are treated as a different population and calculated in separate simulation runs since their abundance is considerably less certain. They are also of the NFW form, but they are truncated. The truncation is done by using the standard approximation to the tidal radius

$$r_t(m, R) = \frac{R m^{1/3}}{(M(R)[3 - \alpha])^{1/3}} ; \alpha \equiv \frac{\partial \ln M}{\partial \ln R} \quad (6)$$

where  $R$  is the distance from the center of the host halo,  $M(R)$  is the mass of the host within that distance and  $m$  is the mass of the subhalo. For the purposes of calculating the tidal radius, the host is taken to be a SIS and  $R$  is set to 5 times the Einstein radius of the host lens. Since not much is known about the mass function of substructures inside a host halo in this mass range, it was decided to use substructures of just one mass at a time and adjust the total surface density of them. This makes interpretation of the results more straightforward.

In addition to the substructure, a model for the host lens must be chosen. The substructure will change the positions of the images slightly so if a lens model is chosen to fit the observed image positions perfectly it will not fit them perfectly after the substructure is added. To produce a perfectly consistent lens model one would have to adjust the host lens model for each realization of the substructure. This is very computationally expensive and not necessary in practice. The shifts in positions are generally small when the masses of the substructures are small ( $\lesssim 0.1''$  for  $m < 10^8 M_{\odot}$ ) and, in addition, since the host lens model is degenerate it is ambiguous how it should be adjusted to correct for the shift. The goal here is to reproduce all the significant characteristics of the observed lens – image configuration, rough image opening angle (within  $2^\circ$ ), redshifts of source and lens – so that one can determine whether lenses look like the ones observed and have the observed ratio anomalies are common in the  $\Lambda$ CDM model.

Often, when the host lens model is set up to produce an extreme cusp or fold caustic configuration and the substructure includes masses of  $\gtrsim 10^8 M_{\odot}$ , the image configuration will be changed so that two of the images are no longer present. In the statistical studies presented in section 6 these cases are simply ignored on the basis of their being incompatible with the lens systems that are being modeled.

### 5.1. comparison with cross section method

Another way to calculate the magnification probability distribution is to use a cross section or optical depth method. This approach significantly reduces the computational work necessary. The magnification as a function of source position is calculated for one subhalo and the host lens is represented by a constant background shear and smooth surface density. From this the cross section,  $\sigma(\mu)$ , is found for a single halo. The probability of getting a magnification of above  $\mu$  is then approximated as  $\tau(\mu) = \eta \sigma(\mu)$  where  $\eta$  is the number density of halos. Keeton (2003) found an analytic approximation to  $\sigma(\mu)$  for a untruncated SIS halo and a point-like source. Chen, Kravtsov, & Keeton (2003) used this result to estimate the influence of halos inside and outside of the primary lens on QSO magnification anomalies.

This method has several drawbacks. Firstly, the cross section approach is only valid for rare events. A typical source will lie roughly equidistant between subhalos; the assumption that the magnification can be calculated using a single subhalo will be valid in only a minority of cases. This would be acceptable if the subhalos were very sparse and the majority of sources were unaffected by them. This is generally not the case however. A typical line of sight out to  $z = 2$  passes within one virial radius of approximately 300 halos with masses between  $10^7 M_\odot$  and  $10^9 M_\odot$ . The standard deviation in the total convergence and shear caused by these halos is on the order of several percent which will cause changes in the magnifications of the sizes seen in these simulations (see Metcalf 2004).

Another problem is that to simplify the calculation in this method the source is taken to be infinitely small compared to the subhalo. This is not a good approximation for a radio or mid-IR source which can be larger than the subhalos under consideration. The subhalo is also taken to be untruncated which will clearly not be the case, especially near the center of the primary lens. Even if the lensing were not sensitive to the truncation radius, it would affect the conversion between subhalo number density and mass density.

The cross section method can also breakdown because the deflections caused by the primary lens are not well approximated by a simple shear and convergence. This is particularly true near the caustics which are of special interest here. Also, the substructure is taken to influence each image independently in the cross section approach. This is not always the case, especially when the images are close together. For example, a single subhalo, if large enough ( $\sim 10^{10} M_\odot$ ) can shift the position and shape of a cusp caustic, changing the positions of all three close images.

The analytic cross section of Keeton (2003) has been used to test the lensing code used in this paper. The code should return the same results when there is only one untruncated subhalo and the source is made very small. This was done for the local shear and convergences appropriate for the 4 images of Q2237+0305. Good agreement was found for  $\Delta\mu > 0.03$  mag below which the finite size of simulated region became important.

## 6. Results

Simulations were performed to mimic the observed lenses discussed in section 4 with the addition of  $\Lambda$ CDM substructure. The resulting combinations of image magnifications are then compared with those observed to determine if the observed anomalies are expected to be reasonably common in this cosmological model.

To represent lens Q2237+0305, and other lenses in the Einstein cross configuration, a host lens model is constructed that fits the image positions of Q2237+0305. The model consists of a

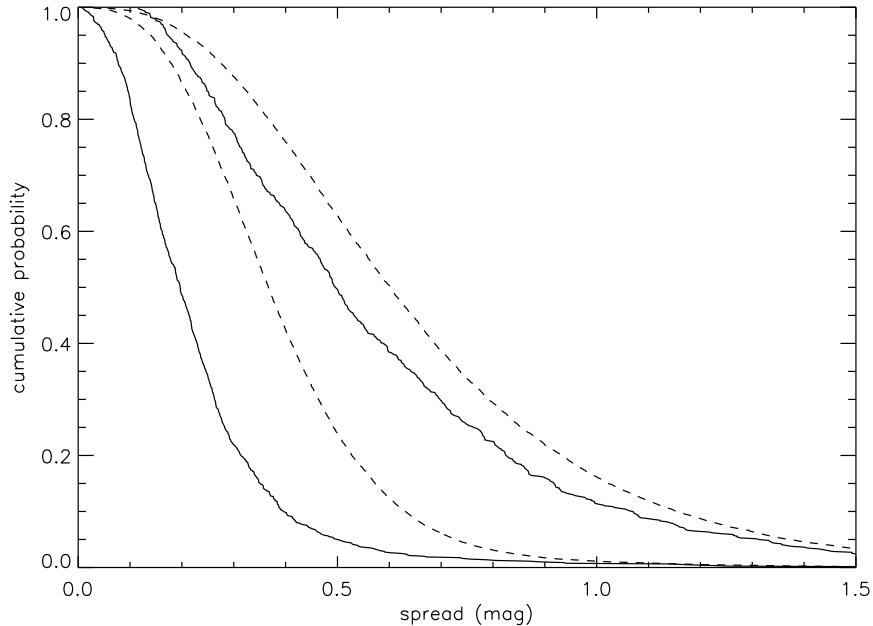


Fig. 2.— This is the probability of having a magnification ratio disagree with the lens model by more than a certain magnitude for Q2237+0305. The two solid curves are without observational noise and the dashed curves are with 0.15 mag of noise. For each type of curve the one on the left is for intergalactic halos with  $10^7 M_\odot < m < 10^8 M_\odot$  and the one on the right is for  $10^7 M_\odot < m < 10^9 M_\odot$ . There is no substructure inside the primary lens.

Singular Isothermal Ellipsoid (SIE) with an external shear and fits the image positions very well. The effects of substructure within the host lens and its contributions to spectroscopic lensing were investigated in Metcalf et al. (2004). Just the intergalactic contribution is discussed here. All the halos within 2 arcsec of the center of the lens are included in the simulations.

For each realization of the substructure the three magnification ratios can be compared with the ratios expected from the host lens model. Figure 2 shows a cumulative distribution of the largest discrepancy (in magnitudes) out of these three between the model and simulated values. The source size is 1 pc in this case. By comparing the curves figure 2 it is found that most of the anomalies are caused by the high end of the mass distribution,  $m \simeq 10^8 - 10^9 M_\odot$ . One can see that these discrepancies are rather large even without any substructure in the host lens itself. Discrepancies as large as  $\sim 0.5$  mag are expected in half the cases. The typical discrepancies between observed flux ratios and models are a few tenths of a magnitude (see Metcalf & Zhao 2002; Kochanek & Dalal 2004). This makes the observed ratio anomalies consistent with  $\Lambda$ CDM, simple lens models and no substructure internal to the primary lenses.

Although figure 2 demonstrates a consistency with  $\Lambda$ CDM it is not certain that CDM substructures are the only possible explanation for the discrepancies in Einstein cross lenses. Some of the discrepancy could be accounted for by a less than perfectly symmetric host lens. Although this probably cannot account for all of the discrepancies, it can significantly change the amount of substructure that is required to produce them and thus it is not a strong constraint on the  $\Lambda$ CDM model.

As described in section 3.2, a more restrictive test comes from the spectroscopic lensing

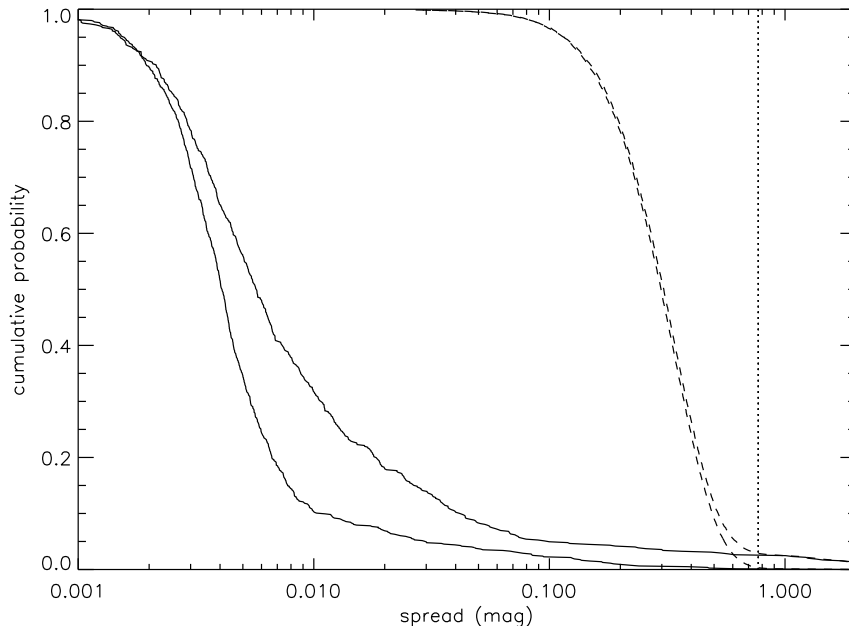


Fig. 3.— The solid curves are the probability of the spread in the differential magnification ratios being above a certain magnitude for Q2237+0305. The source sizes used are 1 pc and 100 pc. The substructure mass ranges are  $10^7 M_\odot < m < 10^8 M_\odot$  for the left most curve and  $10^7 M_\odot < m < 10^9 M_\odot$  for the solid curve on the right. The dashed curves are the same but with 0.15 mag of noise which was the level measured in Metcalf et al. (2004). The dotted line marks the measured discrepancy between the radio/mid-IR magnification ratios and the narrow line magnification ratios reported in that paper.

observations of Q2237+0305. Figure 3 shows the cumulative distribution of the spread in the differential magnification ratios between a 100 pc source and a 1 pc source. These are very small; much smaller than the spread of  $0.77 \pm 0.15$  mag between the narrow line emission region and the mid-IR emission region measured by Metcalf et al. (2004). CDM halos seem easily capable of changing the magnification ratios by this much, but they do not produce the mismatch in the magnifications of different size sources. This problem can be traced to a deficiency of small mass ( $\sim 10^6$ ) halos in the  $\Lambda$ CDM model. As we shall see this is the only strong inconsistency between the  $\Lambda$ CDM model and magnification ratio measurements.

In considering the case of B1422+231 the same kind of simulations are performed only the cusp caustic parameter,  $R_{\text{cusp}}$ , is calculated for each realization. The host lens is again a SIE+shear model fit to the observed image positions. Figure 4 shows the distribution of  $R_{\text{cusp}}$  with the expected population of intergalactic halos only. The first thing to note is the marked asymmetry in the distribution. As previously seen (Metcalf 2001; Metcalf & Madau 2001; Schechter & Wambsganss 2002), the magnifications of negative magnification images are affected by substructure differently than positive magnification images. When substructure is added,  $R_{\text{cusp}}$  should be biased toward positive values as seen here.

Also shown in figure 4 is the observed value of  $R_{\text{cusp}}$  for comparison. There is a perfectly reasonable probability of  $\simeq 0.28$  that  $R_{\text{cusp}}$  would be even larger than the observed value. By comparing the two different ranges for the halo masses, it can be seen that violations in the cusp caustic relation are mostly caused by more massive halos in this case. Also note that a

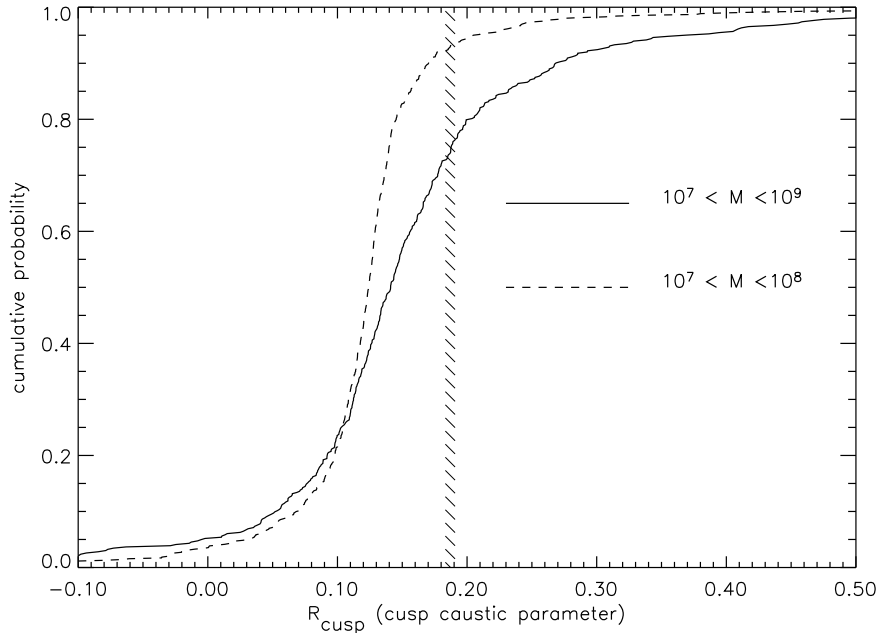


Fig. 4.— The distribution of the cusp caustic parameter,  $R_{\text{cusp}}$ , for lens B1422+231 with only intergalactic standard  $\Lambda$ CDM small-scale structure. The observed value in the radio with error is shown as the hashed region. The different curves correspond to the halo mass ranges shown. It can be seen that most of the changes in  $R_{\text{cusp}}$  are caused by relatively large mass halos,  $10^8 M_{\odot} < m < 10^9 M_{\odot}$ . There is about a 25% chance of  $R_{\text{cusp}}$  differing from zero by more than is observed.

negative  $R_{\text{cusp}}$  of the same magnitude would be clearly inconsistent with this explanation. In light of this, the violation of the cusp caustic relation in B1422+231 seems fully consistent with the  $\Lambda$ CDM model even without substructure within the halo of the primary lens.

We can also compare figure 4 to lens B0712+472 which has a similar configuration to B1422+231 although a lower source redshift. It is easily seen that its value of  $R_{\text{cusp}} = 0.26 \pm 0.02$  is not particularly unlikely (there is a  $\sim 12\%$  probability of it being larger) and thus does not require an additional explanation beyond the expected population of intergalactic halos. Considering the additional substructure within the host lens, the observed  $R_{\text{cusp}}$  seems perfectly consistent with  $\Lambda$ CDM. Although a precise calculation would require modeling this particular lens specifically, the results would not change greatly if that was done.

Lens B2045+265 is a more extreme cusp caustic case. When the source is very near the cusp, substructure can have a significant effect on the details of the lens configuration such as the precise image opening angle. After substructures are added to a host lens model, the image positions will not fit the observed ones precisely, but the lens will still be very similar in its general aspect. To investigate the violations of the cusp caustic relation in cases like this, a SIS+shear host lens model is constructed that reproduces the approximate size and image opening angle of B2045+265. The image configuration for this model is shown in figure 5.

Figure 6 shows the results for simulations with just intergalactic  $\Lambda$ CDM halos. Also shown is the observed value for  $R_{\text{cusp}}$ . With a halo mass range of  $10^6 M_{\odot} < m < 10^9 M_{\odot}$  the observed  $R_{\text{cusp}}$  does not appear strongly disfavored – 15% chance of it being larger. Again one sees the strong asymmetry of the distribution. An observed value of  $R_{\text{cusp}} \lesssim -0.3$  would have been

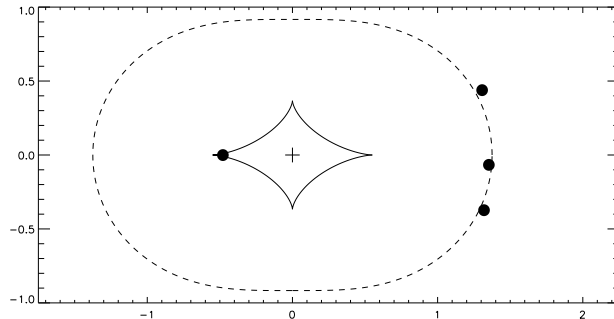


Fig. 5.— Diagram of the close cusp caustic model used in simulations. The dots are where the centers of the images are and the + marks the center of the lens. The units are in arcseconds. The image opening angle is  $25.5^\circ$ . The redshifts used are the same as for B2045+265,  $z_{\text{lens}} = 0.87$  and  $z_{\text{source}} = 1.28$ .

strong evidence against the substructure explanation for the magnification ratio anomalies.

The importance of substructures within the host lens for a B2045+265–like lens was also investigated. For the  $10^9 M_\odot$  and  $10^8 M_\odot$  cases the range was 2 arcsec from the center of the lens. Because of the high number of individual subhalos in the  $10^7 M_\odot$  case the range was reduced to the 1.61 arcsecs surrounding the image triplet. Figure 7 shows the results for different substructure masses and surface densities. For a host lens with a radial profile similar to a SIS ( $\rho(r) \propto r^{-2}$ ), the Einstein radius – and thus the images – forms where  $\kappa \simeq 0.5$ . For this reason we expect a substructure surface density of  $\kappa = 0.005$  to be  $\sim 1\%$  of the total surface density in the lens. From figure 7 it can be seen that this is enough substructure to account for the observed  $R_{\text{cusp}}$  if the mass scale is  $\sim 10^8 M_\odot$  or greater. Substructure within the primary lens could be the most significant cause of the anomaly in this case, but comparing figure 6 to figure 7 shows that the contributions from internal and external substructure are comparable.

The importance of intergalactic halos will come as a surprise to some. Calculating some simple numbers can make it less so. The total  $\kappa$  (surface density weighted by the critical density) in halos below  $10^9 M_\odot$  along a line of sight to  $z = 2$  is  $\sim 0.15 - 0.19$ . The variance in this number is  $\langle \kappa^2 \rangle^{1/2} \simeq 0.04$  with the halo model used here. This is close to 10% of the surface density of the primary lens, larger than the expected level needed to cause the monochromatic magnification anomalies.

## 7. Discussion

It has been shown here that anomalies in the monochromatic (as opposed to differential) magnification ratios of cusp caustic lenses might be explained naturally within the  $\Lambda$ CDM model with little if any substructure within the dark matter halo of the primary lenses. Intergalactic halos could be enough to account for these anomalies. This conclusion is derived from simulating several realistic and representative cases where it is shown that the cusp caustic relation is violated by such halos. Furthermore, the typical observed anomalies in the monochromatic

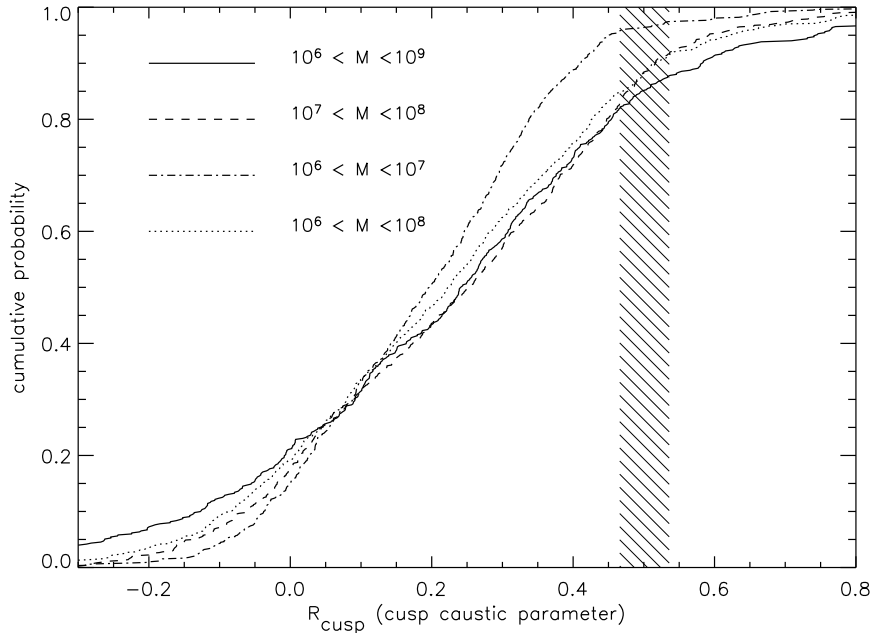


Fig. 6.— The cumulative distribution for  $R_{\text{cusp}}$  in the tight long axis case like B2045+265 with only intergalactic substructure. The observed value of  $R_{\text{cusp}}$  in the radio is shown by the hashed region. The included subhalo mass ranges are shown.

magnification ratios of several tenths of magnitudes – when compared to simple lens models – are easily explained in the same way. The contribution to flux anomalies from intergalactic halos is found to be significant. Measuring the amount of substructure that is within the primary lens halos for comparison with Nbody simulations will require a large number of lenses and an accurate prediction for the intergalactic contribution. These anomalies in the monochromatic magnification ratios could also be explained by smaller scale structures since they do not provide significant constraints on the substructure mass. The fact that all of the observed cusp caustic parameters,  $R_{\text{cusp}}$ , are positive is further support for the conclusion that these anomalies are being caused by some kind of substructure.

The alternative to intergalactic halos, substructure in the primary lens, could also be contributing to the magnification ratio anomalies although the expected abundance of such substructures is not yet certain. Mao et al. (2004) have argued that Nbody simulations indicate that there is not enough substructure in  $\Lambda$ CDM halos to explain the lensing observations. This argument requires extrapolating the mass function of subhalos beyond the limitations of the current simulations to smaller masses and further into the centers of the halos. For this reason, it cannot yet be determined if the additional intergalactic halos cause magnification anomalies to be overabundant relative to observations.

Chen et al. (2003) found that intergalactic halos play a significant, but less important role in the magnification anomalies. The disagreement with this paper appears to be a result of Chen et al. (2003) not taking into account of deflections by multiple halos and approximating the host lens as a simple shear and constant surface density instead of modeling it in more detail (see section 5.1). The collective surface density in small, intergalactic halos is significant and varies across the sky. These perturbations in the surface density are enough to change the image



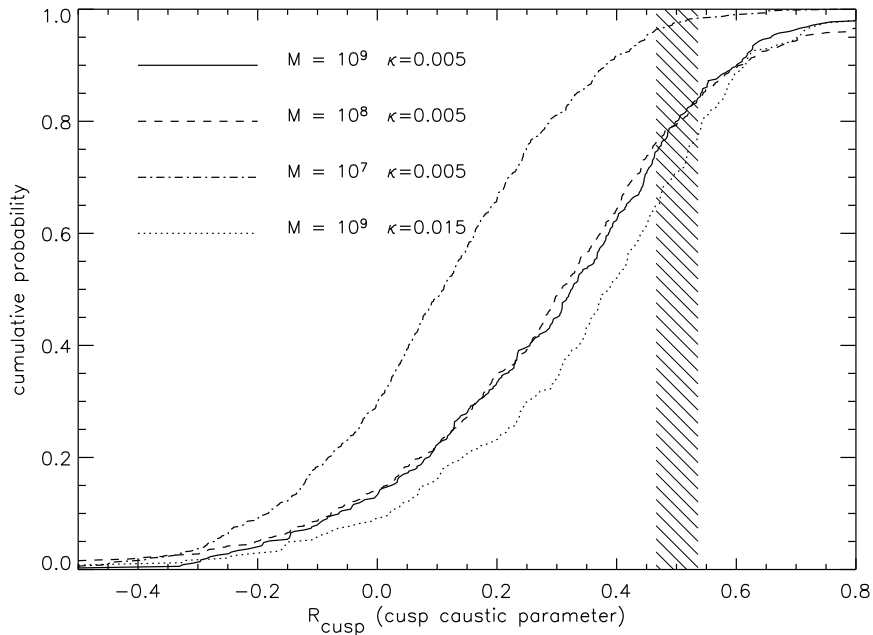


Fig. 7.— The cumulative distribution for  $R_{\text{cusp}}$  in a tight long axis case like B2045+265 with substructure inside the host lens. In each case the subhalos are of the mass as indicated. The total average surface density in substructure is indicated in units of the critical density. A surface density of  $\kappa = 0.005$  is approximately 1% of the surface density. The observed value and errors are indicated by the hash marks.

magnifications by tenths of a percent.

In contrast to the monochromatic magnification ratios, the spectroscopic gravitational lensing observations of Q2237+0305 require more small mass halos than are expected in the  $\Lambda$ CDM model. Bent multiply imaged radio jets also hint, although less securely, at a large number of small mass objects (Metcalf 2002). The case for small mass substructure is not yet secure, but further data should resolve the issue. On the theoretical side, advances in cosmological simulations should soon make it possible to extend predictions for the mass function of substructures within the halos of large galaxies down to smaller masses and smaller galactocentric radii where they can be more directly compared with observations. At this time, there is an inconsistency between the  $\Lambda$ CDM model and the gravitational lensing observations that needs to be resolved.

The author would like to thank J. Bullock for very useful discussions and M. Magliocchetti for very helpful suggestions. I would also like to thank J. Primack and his group for allowing me to use their beowulf computer cluster. Financial support was provided by NASA through Hubble Fellowship grant HF-01154.01-A awarded by the Space Telescope Science Institute, which is operated by the Association of Universities for Research in Astronomy, Inc., for NASA, under contract NAS 5-26555

## REFERENCES

- Andreani, P., Franceschini, A., & Granato, G. 1999, MNRAS, 306, 161
- Bennert, N., Falcke, H., Schulz, H., Wilson, A. S., & Wills, B. J. 2002, ApJ, 574, L105
- Bradač, M., Schneider, P., Steinmetz, M., Lombardi, M., King, L. J., & Porcas, R. 2002, A&A, 388, 373
- Chen, J., Kravtsov, A. V., & Keeton, C. R. 2003, ApJ, 592, 24
- Chiba, M. 2002, ApJ, 565, 17
- Dalal, N. & Kochanek, C. S. 2002, ApJ, 572, 25
- De Lucia, G., Kauffmann, G., Springel, V., White, S. D. M., Lanzoni, B., Stoeck, F., Tormen, G., & Yoshida, N. 2004, MNRAS, 348, 333
- Evans, N. W. & Witt, H. J. 2003, MNRAS, 345, 1351
- Fassnacht, C. D., Blandford, R. D., Cohen, J. G., Matthews, K., Pearson, T. J., Readhead, A. C. S., Womble, D. S., Myers, S. T., et al., 1999, AJ, 117, 658
- Hayashi, E., Navarro, J. F., Taylor, J. E., Stadel, J., & Quinn, T. 2003, ApJ, 584, 541
- Irwin, M. J., Webster, R. L., Hewett, P. C., Corrigan, R. T., & Jedrzejewski, R. I. 1989, AJ, 98, 1989
- Jackson, N., Nair, S., Browne, I. W. A., Wilkinson, P. N., Muxlow, T. W. B., de Bruyn, A. G., Koopmans, L., Bremer, M., et al., 1998, MNRAS, 296, 483
- Kaspi, S., Smith, P. S., Netzer, H., Maoz, D., Jannuzi, B. T., & Givon, U. 2000, ApJ, 533, 631
- Keeton, C. 2002, preprint, astro-ph/0112350
- Keeton, C. R. 2003, ApJ, 584, 664
- Keeton, C. R., Gaudi, B. S., & Petters, A. O. 2003, ApJ, 598, 138
- Klypin, A., Kravtsov, A. V., Valenzuela, O., & Prada, F. 1999, ApJ, 522, 82
- Kochanek, C. S. & Dalal, N. 2004, ApJ, 610, 69
- Koopmans, L. V. E., Biggs, A., Blandford, R. D., Browne, I. W. A., Jackson, N. J., Mao, S., Wilkinson, P. N., de Bruyn, A. G., et al., 2003, ApJ, 595, 712
- Mao, S., Jing, Y., Ostriker, J. P., & Weller, J. 2004, ApJ, 604, L5
- Mao, S. & Schneider, P. 1998, MNRAS, 295, 587
- Metcalf, R. 2001, in Where is the Matter?, ed. L. Tresse & M. Treyer (astro-ph/0109347)
- Metcalf, R. B. 2002, ApJ, 580, 696
- Metcalf, R. B. 2004, preprint, submitted to ApJ
- Metcalf, R. B. & Madau, P. 2001, ApJ, 563, 9
- Metcalf, R. B., Moustakas, L. A., Bunker, A. J., & Parry, I. R. 2004, ApJ, 607, 43
- Metcalf, R. B. & Zhao, H. 2002, ApJ, 567, L5
- Moore, B., Ghigna, S., Governato, F., Lake, G., Quinn, T., Stadel, J., & Tozzi, P. 1999, ApJ, 524, L19
- Moustakas, L. A. & Metcalf, R. B. 2003, MNRAS, 339, 607

- Navarro, J. F., Frenk, C. S., & White, S. D. M. 1997, *ApJ*, 490, 493
- Patnaik, A. R. & Narasimha, D. 2001, *MNRAS*, 326, 1403
- Press, W. H. & Schechter, P. 1974, *ApJ*, 187, 425
- Richards, G. T., Keeton, C. R., Pindor, B., Hennawi, J. F., Hall, P. B., Turner, E. L., Inada, N., Oguri, M., et al., 2004, *ApJ*, 610, 679
- Rusin, D., Norbury, M., Biggs, A. D., Marlow, D. R., Jackson, N. J., Browne, I. W. A., Wilkinson, P. N., & Myers, S. T. 2002, *MNRAS*, 330, 205
- Saha, P. & Williams, L. L. R. 2003, *AJ*, 125, 2769
- Schechter, P. L. & Wambsganss, J. 2002, *ApJ*, 580, 685
- Schneider, P., Ehlers, J., & Falco, E. E. 1992, *Gravitational Lenses* (Springer-Verlag)
- Schneider, P. & Weiss, A. 1992, *A&A*, 260, 1
- Sheth, R. K. & Tormen, G. 2002, *MNRAS*, 329, 61
- Sluse, D., Surdej, J., Claeskens, J.-F., Hutsemékers, D., Jean, C., Courbin, F., Nakos, T., Billeres, M., et al., 2003, *A&A*, 406, L43
- Taylor, J., Silk, J., & Babul, A. 2004, in *Dark Matter in Galaxies*, ed. S. Ryder, D. Pisano, M. Walker, & K. Freeman, ASP Conference Series
- Taylor, J. E. & Babul, A. 2001, *ApJ*, 559, 716
- . 2004, *MNRAS*, 348, 811
- Wambsganss, J., Schneider, P., & Paczynski, B. 1990, *ApJ*, 358, L33
- Wandel, A., Peterson, B. M., & Malkan, M. A. 1999, *ApJ*, 526, 579
- Winn, J. N., Rusin, D., & Kochanek, C. S. 2004, *Nature*, 427, 613
- Wisotzki, L., Becker, T., Christensen, L., Helms, A., Jahnke, K., Kelz, A., Roth, M. M., & Sanchez, S. F. 2003, *A&A*, 408, 455
- Woźniak, P. R., Alard, C., Udalski, A., Szymański, M., Kubiak, M., Pietrzyński, G., & Zebruń, K. 2000, *ApJ*, 529, 88
- Wyithe, J. S. B., Agol, E., & Fluke, C. J. 2002, *MNRAS*, 331, 1041
- Wyithe, J. S. B., Webster, R. L., & Turner, E. L. 2000, *MNRAS*, 318, 762
- Yonehara, A. 2001, *ApJ*, 548, L127
- Zentner, A. R. & Bullock, J. S. 2003, *ApJ*, 598, 49